https://doi.org/10.5194/se-2020-11
Preprint. Discussion started: 19 February 2020

Solid Earth
Discussions
Open Access
EGU

The abyssal giant pockmarks of the Black Bahama Escarpment: Relations between structures, fluids and carbonate physiography

Thibault Cavailhes[1], Hervé Gillet[1], Léa Guiastrennec-Faugas[1], Thierry Mulder[1], Vincent Hanquiez[1]

[1] Université de Bordeaux (UMR EPOC – OASU CNRS 5805) Allée Geoffroy Saint-Hilaire CS 50023 33615 Pessac, France

Correspondence to: Thibault Cavailhes (thibault.cavailhes@u-bordeaux.fr)

Abstract.

This study reports the discovery of spectacular abyssal giant pockmarks located at the toe of the Bahamian carbonate platform, along the Black Bahama structurally-controlled Escarpment (BBE) that exhibits up to 4 km of submarine elevation above the San Salvador Abyssal Plain (SSAP). Analysis of seismic reflection and bathymetric data collected during the *CARAMBAR 2 cruise* revealed the presence of 29 pockmarks; their water depths range from - 4584 m to -4967 m whereas their bathymetric depressions are elliptical in shape, range in diameter from 255 m to 1819 m, and in depth from 30 m to 185 m. The pockmarks alignment trends parallel to the BBE as well as the structural lineaments of the area, exclusively between 2200 and 5000 m from its toe, and overlies a buried carbonate bench in which a high-amplitude seismic anomaly has been detected. The pockmark density interestingly increases where the recognized structural lineaments intersect the BBE.

The aforementioned observations suggest an atypical relationship between the spatial occurrence of the abyssal fluid releases, the carbonate platform tectonic structures, the buried carbonate bench that underlies the hemipelagites in the San Salvador abyssal plain and the physiography of the area. Indeed, the ground water entrance during low-level stands, the dissolution of evaporites by meteoric water, the platform-scale thermal convection and the seawater entrance at the platform edge most probably act in concert to favor the circulation of brines and therefore the corrosion within the Bahamian carbonate platform. These mechanisms are particularly efficient along the structural heterogeneities (i.e. faults and fractures) which act as fluid conduits and control the physiography of the area by maintaining the location of the sedimentary pathways. The dense fluids migrate along the faults towards the BBE free edge and are subsequently trapped into the buried carbonate bench that laterally disappears below the low-permeability deep-sea hemipelagics of the SSAP. In consequence, the trapped corrosive fluids dissolve the carbonates preferentially along the tectonic structures such as the Samana Fracture Zone, at the origin of the BBE curvature and triggers collapse-structures in the overlying fine-grained deposits generating giant pockmarks. This structurally-directed process of dissolution is believed to have played a major role in the BBE 5-6 km erosional retreat and also probably explains the occurrence of plunge pools in the area.

https://doi.org/10.5194/se-2020-11
Preprint. Discussion started: 19 February 2020

Solid Earth
Discussions
Open Access
EGU

1. Introduction

Localizing, describing and understanding the zones of the upper crust where the fluids enter, flow, are stored and leak, are critical to discuss and quantify the geo-bio-chemical fluxes between the lithosphere, the hydrosphere and the atmosphere of the Earth (e.g. Dickens, 2003). Since the 1970's, our 4D-conception of the upper crust fluid circulation has been significantly improved by the description and the analysis of submarine fluid-escape features distribution and morphologies (e.g. King and Mac Lean, 1970; Hornbach et al., 2007). Firstly, seafloor seepages have major impacts on seabed stability, implying potential hazards to offshore infrastructures as well as to coastal infrastructures by changing the failure rock mechanics that potentially leads to submarine escarpment destabilization and possibly to tsunamis (e.g. Orange et al., 2002 and herein references). Secondly, their distribution affine our knowledge of the freshwater distribution, storage and flows in coastal and marine systems where the freshwater supply to cities remains problematic (Garven and Freeze, 1984; Post et al., 2013). Thirdly, fluid-escape features distribution has also helped the oil and gas exploration geologists, which have used their presence to detect offshore seepages related to underlying petroleum systems since the 1930's (Abrams and Segall, 2001). Lastly, long-term seeping fluids through the seafloor has been identified as the primary energy for chemosynthetic benthic ecosystems that currently localize a poorly understood submarine high biomass and productivity (Dando et al., 1991; Ondréas et al., 2005).

Pockmark definition

King and Mac Lean (1970) first defined the structures discovered off Nova Scotia as follow "*Pockmarks are cone-shaped depressions… possibly formed by ascending gas or subsurface water leakage from underlying … sediments*". These crater-like features commonly occur in fine-grained sediments, have circular to ellipsoidal depression shapes and can reach up to 4000 m in diameter (Cole et al., 2000; Michaud et al. 2005). They have been observed in all ranges of water depth, from shallow-water environments (e.g. ~ -10 m, Backshall et al., 1979) to deep-sea water (~ -3160 m in Marcon et al., 2014) and are considered as giants pockmarks in the case their diameter is greater than 250 m (Foland et al., 2007; Pilcher and Argent, 2007). They have been recognized in different settings such as open oceanic environment (Michaud et al., 2005), lakes (e.g. Chapron et al., 2004), active margins (Salmi et al., 2011), passive margins (Ondréas et al., 2005), along a volcanic ridge (Michaud et al., 2005), in clastic environments (Sultan et al., 2010), in carbonate environments (Backshall et al., 1979; Betzler et al., 2011) and even proposed for explaining some observed Mars surface circular morphologies (Komatsu et al., 2011). Rare fossil palaeo pockmarks have been described in outcrop studies such as the ones from Cantabria in Spain or the southeast basin of France (e.g. Agirrezabala et al., 2013; Gay et al., 2019).

The fluid sources related to pockmarks commonly originate from shallow subsurface sediments (e.g. Baltzer et al. 2017), dewatering and degassing of the gas-charged seafloor (Agirrezabala et al., 2013), buried salt diapirs (e.g. Taylor et al., 2000; Gay et al., 2019), drowned carbonate banks (e.g. Betzler et al., 2011), buried unconformities (e.g. King and MacLean, 1970), buried sedimentary channels (Picher et al., 2007; Gay et al., 2003; Ondreas et al., 2005), buried Mass Transport Deposits (Bayon et al., 2009) and/or underlying petroleum systems (Pilcher and Argent, 2007). The nature of the involved-fluids can be of various origins such as biogenic gas (e.g. Cole et al., 2000; Marcon et al., 2014), thermogenic gas such as hydrates (Pilcher and Argent, 2007), hydrocarbons

https://doi.org/10.5194/se-2020-11
Preprint. Discussion started: 19 February 2020


Solid Earth
Discussions
Open Access
EGU

seeps and/or sand injectites (Cole et al., 2000), fresh water (Chapron et al., 2004) as well as brines and sulfides (Paull and Neumann, 1987).

The fluid ascending movements giving birth to pockmarks can be favored along structural surfaces or rocky basements (Shaw et al., 1997), through fractures in the sediments (e.g. Marcon et al., 2014) and through fault-zones of different scales (e.g. Sultan et al., 2010; Micallef et al., 2011). Fault-strike pockmarks is the relevant terminology for the linear arrangement of pockmarks along the strike of an underlying buried fault (Pilcher and Argent, 2007) whereas fault hanging-wall pockmarks are located above the footwall cut-offs of a fluid-rich unit (Maestro et al., 2002).

Current-day carbonate platforms are commonly subject to dissolution, corrosion, dolomitization and dedolomitization by fresh and saline groundwater in the first kilometers deep (e.g. Sanford and Konikrow, 1989; Hugues et al., 2007; Wierzbicki et al., 2006). The structural heterogeneities are the most efficient fluids entrance, pathway, storage and seepage available spaces in carbonate rocks, allowing both episodic and persistent subsurface fluid-flows through times and overprinting an anisotropy of hydraulic properties in the system, notably the permeability (Sibson, 1996). At the cm-scale, preexisting fractures and faults control the distribution, the orientation and the intensity of the carbonate dissolution by the circulating brines (defect-driven kinetic reactions); the channelized shape of dissolution targets fractures and zones of structural weakness, preferentially along their strikes (Gouze et al., 2003; Garcia-Rios et al., 2015; Privalov et al., 2019). The structurally-controlled dissolution of carbonates, in particular by brines, is poorly understood and remains to be documented at the km-scale.

The Bahama platform offers within a same succession many reservoir rocks with a wide range of porosities (thick shallow water platform limestones and dolomites), organic matter-rich source rocks (restricted marine limestones) as well as the presence of vertical and lateral seals (thick restricted marine anhydrites and restricted marine halites), all needed for petroleum systems (Walles, 1993). In addition, the Black Bahama Escarpment (BBE) offers a 4 km-high submarine topography that increases the vertical interacting section between groundwater and seawater, where the structural lineaments sharply dissect and controls the submarine physiography. This provides an ideal study case to better constrain a structurally-controlled and dissolved carbonate system at the >km-scale. Indeed, evidences such as significant changes in temperature around faults demonstrate the direct and efficient hydrologic relations between surface and great depths (3500 m) into the platform (Walles, 1993). Drilling and core data show that hydrodynamic alteration processes in carbonates near major fault surfaces create buried dissolution conduits (e.g. 8 meters high, $\phi = 100\%$) at a depth of 4000 meters in the Great Bahama Bank (Walles, 1993). Solution collapse brecciation of dolomite sequences, in response to the dissolution of imbedded anhydrites by corrosive fluids along faults, are suspected to cause those surprising reservoir properties within the platform.

In this paper, (i) we address the distribution, the morphometry and the different mechanisms at the origin of the spectacular abyssal giant pockmarks alignment located at the toe of the BBE (Fig. 1). In doing so, we use the bathymetric/seismic data of CARAMBAR 2.0 scientific cruise (December 2016-January 2017) in order to (ii) document and discuss the interactions between the km-scale structural features of the area, the carbonate platform-scale circulation and the current-day physiography. To our knowledge, pockmarks have never been described on modern sea-floor below the Carbonate Compensation Depth (CCD), in abyssal carbonate contexts (>3000 m of water depth), at the toe of a structurally-controlled mega-carbonate escarpment such as the BBE (> 4 km-high).

https://doi.org/10.5194/se-2020-11
Preprint. Discussion started: 19 February 2020

2. Geological setting

2.1 Tectonic setting and platform establishment

The Bahamas is a post-rift feature mostly made of a stretched pre-Triassic continental crust (Mullins and Lynts, 1977) where a large carbonate platform developed in the Late Jurassic and Early Cretaceous in response to high carbonate production rates (Freeman-Lynde et al., 1981; Carlo, 1996). The clockwise rotation of the North American continental structural block caused a complex transtensional ocean-continent transition where N-S striking normal basement faults (e.g. Black Plateau) have coexisted with E-W striking pre-Jurassic basement Atlantic Ocean fracture zones (e.g. Blake Spur FZ, Great Abaco FZ; Sheridan, 1974). Since the early Cenozoic, active faulting occurred in response to the tectonic interactions between the southern Cuban orogeny and the Mesozoic-aged tectonic structures (Masaferro et al., 2002; Kindler et al., 2011). Post-Oligocene reactivation of vertical basement faults have been reported by Mullins and Van Buren (1981) in Walker's Cay (northern Bahamas) as well as a Neogene to present-day folding in Santaren anticline (Masaferro et al., 2002) and during the Quaternary-aged tectonic tilting using the Sunniland Fracture Zone along the Bahama escarpment (Kindler et al., 2011; Fig. 1a).

2.2 Current-day physiography and fluid escape features

The present-day morphology of the Blake Bahama Escarpment (BBE) has an erosional origin (~5-6 km of retreat, up to 4.2 km high), essentially developed during the Cretaceous (Freeman-Lynde and Ryan, 1985) and Tertiary times (Schlager et al., 1984), nevertheless the erosion is probably still active. This erosional retreat overprinted a buried "bench-shaped" morphology exhibiting a relict ~5-6 km-wide flat carbonate surface currently buried by Miocene to Quaternary sediments lying in the San Salvador Abyssal plain (Schlager et al., 1984). Consistently to the Blake Escarpment (10-15 km of retreat), an Oligocene unconformity (A^u) is present at the top of the Cretaceous carbonates of the buried-bench and predates the Miocene massive sequences of turbidites and the Quaternary hemipelagites (Paull and Dillon, 1980). Contouritic deposits are present at the toe of the BBE at least since the Oligocene in response to abyssal currents activity Bliefnick et al., 1983; Mulder et al., 2019). The aforementioned erosion at the origin of the BBE would be mainly due to the following mechanisms acting in concert in non-quantified proportion at different times: (i) the circulating saline waters and brines that seep from the base of the escarpment dissolve the carbonates and therefore destabilize the slopes (Walles, 1993; Henderson et al., 1999; Paull and Neumann, 1987), such as described along at least 10% of the Florida carbonate Escarpment base (Paull et al., 1988; Chanton et al., 1991). These are made of 94% of seawater and 6% of dense brines (Chanton et al., 1991) and reach temperatures up to 115°C (Paull and Neumann, 1987). The combination of hydrogen sulfides (HS^-) and oxygenated seawater (from the platform slope) favors acids (H^+) formation that corrode the toe of the escarpment along open vertical fractures. The slope of the escarpment steepens with depth and inner platform carbonate facies at its base strongly suggest that collapse dismantlement operate in depth in response to brine seeps. (ii) Locally, the tectonic activity related to movements along fracture zones implies rock jointing and slope destabilization (Freeman-Lynde and Ryan, 1985).

https://doi.org/10.5194/se-2020-11
Preprint. Discussion started: 19 February 2020


Solid Earth
Discussions
Open Access
EGU

In contrast, the following mechanisms have been interpreted as non-significant to destabilize the slopes of the BBE: (i) the dissolution by oceanic corrosive water below the CCD (Freeman-Lynde and Ryan, 1985) has been excluded by Peterson, (1966) and Paull and Neumann, (1987). (ii) The removal of sediments at the base of the slope by abyssal currents (Schlager et al., 1984; Freeman-Lynde and Ryan, 1985) has been excluded by Paull and Neumann (1987). Indeed, the authors clearly show evidences for such similar erosional structures along the Florida escarpment where the abyssal currents are clearly absent. In addition, (iii) the bioerosion has probably a very limited impact as argued in Freeman-Lynde and Ryan (1985).

2.3 Carbonate platform circulation

Fluids circulation within the Bahamas carbonate platform has operated at different times, involving a wide range of fluid volumes, natures (freshwater, seawater and brines) and mechanisms; this has therefore needed efficient and long-term motors of circulations (Melim and Masaferro, 1997). The fluids circulation in a non-quantified proportion is related to: **(i)** the thermally driven circulation causing density gradients between cold ocean waters and ground waters of the carbonate platform that are warmed by the geothermal heat flux (Kohout et al., 1977; Whitaker and Smart, 1990). **(ii)** The lateral flow due to an across-the-bank head difference (Whitaker and Smart, 1993; Whitaker et al., 1994) and the reflux of mesosaline brines along the platform (salinity of 38-45 ‰) also cause circulation that have important diagenetic implications such as pervasive secondary dolomitization thanks to the magnesium available in the seawater (Simms, 1984; Whitaker and Smart, 1990). The circulation of saline ground water within carbonate platforms is so called the Kohout convection (Hugues et al., 2007). **(iii)** The topographically-driven meteoric groundwater is probably a key factor efficiently driving fluid-circulation into the carbonate platform, in particular during low level stands (Wilson, 2005). The flooding of the banks at the last-deglaciation also strengthened the thermal convection (Dawans and Sawart, 1988; Whitaker et al., 1994). **(iv)** Jointing eases the dissolution by increasing surface area exposed to corrosive waters (Freeman-Lynde and Ryan, 1985) and most probably enhances the existing circulation by supplying efficient, both structurally porous and permeable km-scale fluid-pathways.

3. Methodology and database

New data set was acquired during the Leg 2 of the CARAMBAR 2 cruise from December 2016 to January 2017 onboard the R/V l'Atalante. The survey covered the southern part of Exuma Sound, the Exuma Plateau, the Black Bahama Escarpment (BBE) and the adjacent San Salvador abyssal Plain, including 20.395 km^2 of multibeam bathymetry and backscatter and 2149 km of HR seismic profiles. Bathymetry and backscatter data have been obtained using a Konsberg EM122/EM710 multibeam echo sounder, and the high-resolution (HR) multichannel seismic system uses a 192 channels steamer and related four 35/35 cu in GI air guns (penetration 1-2.5 s two-way travel time). Pockmarks and structural lineaments have been mapped using their physiographic expressions such as depression, local changes in isobaths trends, as well as their seismic expression where 2D seismic data were available (Fig. 2).

4. Results

https://doi.org/10.5194/se-2020-11
Preprint. Discussion started: 19 February 2020


Solid Earth
Discussions
Open Access
EGU

198

199 **4.1 Submarine current-day physiography**

200 The studied area is located on an ocean-continent transition that has been as a transforming ocean-
201 continent passive margin (Mullins et al., 1992; Fig. 1a). The Sunniland Fracture Zone (SFZ) bounding the San
202 Salvador Abyssal Plain (SSAP) is parallel to the oceanic paleo transform faults identified on the sea floor of the
203 North Atlantic Plate (NAP); this major transform tectonic corridor trends perpendicular to the magnetic anomalies
204 of the oceanic crust and sharply controls the Eastern side of the Bahamas submarine physiography (Fig. 1a). Only
205 few morphologies and reliefs of the studied area are simply parallel to the N-S striking tensional basement faults
206 recognized in Sheridan's works (1974) that control the Black Plateau area shape.

207 Based on the analysis of bathymetric maps, the Drowned Barrier Reef (DBR), the Exuma Canyon (EC),
208 the Samana Reentrant (SR), the Exuma Valley (EV), the Exuma Plateau (EP), the South Exuma Plateau Valley
209 (SEPV), the Crooked Canyon (CC), the BBE, the *plunge pools*, and the contouritic deposits have been named
210 consistently to Mulder et al. (2019) (Fig.1b). The generally N-S trending carbonate BBE can reach up to 4200 m
211 of submarine elevation above the San Salvador Abyssal Plain (SSAP) and exhibits an 18 km long curvature located
212 at ~74°10'W; 23.32'N. The BBE curvature is exactly located at the intersection between the SFZ and the BBE.
213 The SFZ appears to be made of different sets of tectonic features, striking N110, N145 and E-W (upper right corner
214 of the figure 1b). The 090E structural lineaments orientation definitely controls the shape of the southern part of
215 the BBE, the northern edge of the Samana Reentrant, the EV and the SEPV. The N110 and N145 trending
216 lineaments (mean ~N130 direction) control the submarine morphologies of the southern edge of the Samana
217 Reentrant (SR), the transition between the EV and the SR, as well as the NW-SE trending BBE curvature (Fig.
218 1b). Regarding the oceanic crust structure in the SSAP, the lineaments are mostly N160 to N-S oriented and
219 controls the elongation of the distal lows where sediments are preferentially deposited (right part of the Figure 1b).
220 In addition, the N-S basement-inherited BBE trend is very similar to the Crooked Canyon orientation. The
221 contourites are present at the toe of the BBE (e.g. Fig. 2a and 2b) with the exception of the BBE curvature area
222 (Fig. 2c).

223 Summarizing these observations, the physiographic sketches of figure 1b reveals that ocean-continent
224 transition inherited structural lineaments control the BBE trends and curvatures, the submarine giant canyon
225 orientations (Mulder et al., 2019) as well as the abyssal topographies, clearly expressed by the structurally-
226 controlled isobaths contours. This is consistent with the conceptual view of Sheridan (1974) arguing for the
227 presence of structural blocks individualizing the Atlantic continental margin by N-S tensional faults and major
228 strike-slip features accommodating block rotation.

229 **4.2 Pockmark Regional distribution**

230 29 abyssal pockmarks have been mapped at the toe of the BBE, in the western part of the SSAP lying at
231 ~ - 4900 m of depth (Fig.1b and 2); they occupy ~20% of the base of the carbonate escarpment, i.e. a total of 21.5
232 km / 102 km long (Fig.1b). Pockmarks depths range from - 4584 m to - 4967 m, exclusively underneath the
233 Carbonate Compensation Depth of the area (~ - 4500 m; Heath and Mullins, 1984) (Fig. 2; Table 1). They are
234 spectacularly all located between 2 km and 5 km seaward of the toe of the BBE (isobath - 4000m). The mean
235 pockmark diameters range from 255 m to 1819 m and form depressions ranging from 30 m to 185 m of depth
236 without any clear preferential direction of elongation (refer to the *4.4 section* for details). The pockmarks of this
237 study (29/29) are so called giant pockmarks considering their diameters wider than 250 m, following the

https://doi.org/10.5194/se-2020-11
Preprint. Discussion started: 19 February 2020


Solid Earth
Discussions
Open Access
EGU

238 classification of Foland et al., (1999). Pockmarks are not randomly distributed in the studied area and show a high
239 concentration nearby the BBE curvature (Fig. 1b and 2c). Pockmarks density increases at the vicinity of the BBE
240 curvature where (i) the structural lineaments of the SFZ intersect the BBE and (ii) where the contouritic deposits
241 are absent. The pockmarks have been classified in two families: the inner pockmarks (n=7; $d_{escarpment}$ = 2 - 3 km)
242 and the outer pockmarks (n=22; $d_{escarpment}$ = 3 - 5 km). In order to facilitate the description of the bathymetric map
243 (Fig.1 and 2), the pockmarks have been numbered from the south to the north (Fig. 2a to 2d); In the case of 14a,
244 14b, 17a and 17b, each couple of overlapping pockmarks have the same number. . This study therefore
245 distinguishes four areas of interest where a detailed analysis of abyssal pockmarks is proposed (Fig. 2a, b, c and
246 d).

247 Pockmark 1 is located in contouritic deposits and clearly appears isolated from the other pockmarks
248 (around 7 km southwards the pockmark 2; Fig.2a and 2b). It seems aligned with the E-W trending structural
249 lineament bounding the north of the EC and the southern *plunge pool* recognized in Mulder et al. (2019) (Fig. 1b).
250 This is also, with the pockmarks 23 to 27, one of the pockmarks of the study piercing contouritic deposits.

251 Pockmarks 2, 4, 6, 7 and to 8 appear to be N-S aligned and located at ~3500 m from the BBE (Fig. 2b).
252 In contrast, the pockmarks 3 and 5 are 1000 m to 2000 m closer to the BBE than 2, 4, 6, and 7. We so call these
253 pockmarks, inner pockmarks (Fig. 2b). The spacing between the pockmarks is comprised between 0 m for the
254 overlapping pockmarks (i.e. #7 and #8) and 1200 m (i.e. #2 and #4).

255 Pockmarks 9, 10, 11, 12, 13, 14a, 14b, 15, 16, 17a, 17b, 18, 19, 20 and 21 are located within the BBE
256 curvature (~74°10'W; 23.32'N; (Fig. 2c). More than half of the studied pockmarks (15/29) are therefore located
257 in the BBE curvature where structural lineaments cross the BBE. Pockmarks 14a, 14b, 17a and 17b are called
258 inner pockmarks because they are located at 2709 m and 2838 m from the BBE (Table 1). In contrast, the other
259 pockmarks form a chain more distant to the BBE (around 4000 m; Fig. 2c). Contouritic deposits seems to be absent
260 from this area (Fig. 1b). Pockmark density is maximum in this area.

261 Pockmarks 22, 23, 24, 25, 26 and 27 are located in the northern part of the studied area where a contouritic
262 body has been mapped (Fig. 1b). The pockmarks water depths range from -4710 m to -4812 m whereas the inner
263 pockmark 26 is located at only 2211 m from the BBE, which contrasts with the others located at around 4000 m
264 from the BBE (Fig. 2d).

265

266 **4.3 Vertical architecture and pockmarks**

267

268 The geological detailed interpretations of seismic profiles in figure 3 are given in figure 4: Both figures
269 have to be read simultaneously. The figure 3a, 3b, 3c, 3d, 3e and 3f respectively correspond to the figure 4a,
270 4b, 4c, 4d, 4e and 4f. These figures exhibits two BBE-perpendicular-trending seismic lines (Fig.3a, 4a and 3d,
271 4d) and one single BBE-parallel trending seismic line (Fig. 3b and 4b), which are all localized in Figure 1.

272 *Sedimentary reflectors* – The offshore seismic reflectors are believed to exhibit respectively from the
273 subsurface to the surface, the top of the oceanic crust (basement), the top Kimmeridgian sedimentary package
274 and the top of the Tithonian sedimentary package, consistently with the work of Schlager et al. (1984) (Fig.
275 3a and 4a). These interpreted sedimentary packages are westwards dipping and thickening, despite the fact
276 their clear seismic expressions is blurring towards the BBE. The oceanic crust is around 0.3 s TWT deep in
277 the eastern part of the profile whereas it is 1.2 s TWT deep in the western part of the profile. Due to this

https://doi.org/10.5194/se-2020-11
Preprint. Discussion started: 19 February 2020

basement structural dip and the high sedimentary supply nearby the platform, the thickness of the sedimentary package is maximum at the toe of the BBE. The Oligocene unconformity (A^u) has also been identified due to its high-amplitude seismic reflections as well as the recognized "downlaps" in the overlying Miocene deep-sea deposits (Fig. 3a and 4a; Paull and Dillon, 1980).

Buried bench - A 6 km wide buried carbonate bench exhibiting a typical blind facies is clearly identifiable in figures 3a and 3d and is similar to the one described for the area (Schlager et al., 1984). The top of this structure is located at around 6.5 s TWT and is overlain by contouritic deposits (Fig. 3a, 4a), except in the BBE curvature surrounding where it lies under a few 200 to 300 ms thick toe of slope hemipelagic cover (Fig. 3d, 3f, 4d and 4f). The seismic signal expression of the bench is also similar to the wider one (10-15 km) recognized at the toe of the Black Escarpment (Paull and Dillon, 1980). Subvertical seismic discontinuities within the bench suggest the presence of well-defined linear, antithetic and therefore "brittle-stylized" collapse faults (Fig. 4c) that have interestingly a "softer" shape in the overlying contouritic body, this latter being probably less lithified than the bench carbonates.

Bright spot - The BBE - parallel seismic line crosses twice the BBE and exhibits diffusive high amplitude seismic anomalies (bright spot) between 6.4 s and 7.0 s TWT. The depth of this feature is independent of the seafloor water depth or relief, therefore demonstrating that this feature originates from subsurface processes (Fig. 3b, 4b). The perpendicular trending seismic line exhibits a V-Shape structure (cone of deformation) which is located right above the buried carbonate bench and terminates on the flank of the pockmark #1. The V-Shape structure is given by antithetic normal faults with sub seismic offsets that form a network apparently accommodating downwards collapse movement (Fig. 3c; 4c)The base of the V-shaped structure is located within the bench (Fig. 3c, 4c), between 0.6 s and 0.9 s underneath the seafloor depression. This bucket-shaped seismic bright spot shows a significant contrast between high-amplitude layered facies recognized in its upper part, the chaotic facies identified at its base and the low amplitude reflectors in the surrounding sedimentary rocks (Fig. 3c, 4c).

Contourites – The fine-grained deep-sea hemipelagics materializes the contouritic body and are crosscut by the pockmark #1 depression (fig. 3c). This depression is bounded by at least four anthithetic curved normal faults and shows a chaotic/disorganized facies in its center. The flanks of the pockmarks, made of at least three packages of contourite deposits, show increasing sedimentary thicknesses at the vicinity of the depression (Fig. 4c). At least the upper package exhibits a hyperbolized seismic facies interpreted as a potential flank destabilization (zoom on fig. 4c).

The 23th of December 2016 (20h13 - 20h23 UT), we recorded with the multibeam echosounder the acoustic response in the water column, in the frame of the Carambar 2 cruise. There was no evidence for acoustic anomalies (fluid plum) in the overlying water columns of the pockmark #1 as well as the 28th of December (15h34 - 15h47 UT), within the water column of the pockmark #15,

4.4 Quantitative analysis

Water depths for the studied pockmarks are comprised between -4584 m and -4967 m (Fig. 5a). The deepest pockmarks are located within the BBE curvature where contouritic deposits are absent. The shallowest pockmark is the southern one (1) that is perched on contouritic deposits and isolated (-4584 m). The inner pockmarks at the vicinity of the BBE curvature (i.e. 14a, 14b, 17a, 17b) are clearly shallower than the outer ones

https://doi.org/10.5194/se-2020-11
Preprint. Discussion started: 19 February 2020


Solid Earth
Discussions
Open Access
EGU

(9, 10, 11, 12, 13, 15, 16, 18, 19, 20, and 21). Consistently, the inner pockmark 26 is shallower than the 24, 25 and 27 outer ones.

All the giant pockmarks of this study are located between 2211 m (#26) and 4648 m (#25) away from isobath "- 4000 m" expressing the toe of BBE in this study (Fig. 5b). The 7 inner pockmarks are located between 2211 m (#26) and 2894 m (#3) from the BBE whereas the outer pockmarks are located between 2943 m (#9) and 4648 m (#25). The greatest distances between the BBE and the outer pockmarks are systematically less than the BBE erosional retreat (5-6 km) proposed in Freeman-Lynde and Ryan, (1985) and Schlager et al. (1980). Pockmarks appear to be always located right above the buried carbonate bench.

Pockmark mean diameters and pockmark shortest distances to the BBE appear dependent according to the positive correlation of the figure 5c. Two main trends can be individualized on this graph, both including inner and outer pockmarks. For both relations, closer from the BBE is the pockmark, smaller it is.

Pockmarks elongations have been measured for outer and inner pockmarks (Fig. 5d). Most of the pockmarks are slightly elongated with the exception of the inner pockmark #5, which probably originated from several underlying coalescent pockmarks. The related rose diagram highlights a slight N-S preferential direction of elongation (Fig. 5d). The inner pockmarks seem to be generally smaller than the outer ones.

The pockmark depression depths positively correlate with the pockmark mean diameters (Fig. 5e). The pockmark depression depths seem to be around 1/10 of the pockmark mean diameters. This scaling law is consistent with the results from Pilcher and Argent (2007).

5. Interpretations and discussion

The physiographic sketch in figure 1 highlights that structural lineaments have most probably controlled and localized through times persistent and well-defined sedimentary pathways from the platform to the San Salvador abyssal plain such as the Great Abaco Canyon (Mulder et al., 2018; 2019). The studied fluid escape features (pockmarks) occupies 20% of the BBE toe and are preferentially localized at the intersection between the BBE and the inherited structural lineaments of the area (Fig. 1a). These observations demonstrate that structurally-driven fluid circulation along the lineaments and through the carbonate platform has probably played a key role during the erosional process leading to the retreat of the BBE. The deep-sea release of fluids have most likely corroded and destabilized the platform toe which is supported by the direct observations that this type of carbonate escarpments currently exhibits unstable submarine slopes steepening with depth (Paull and Neumann, 1987; Fig. 6). The BBE erosional retreat has therefore preferentially reused the inherited faults initially formed by the existing transforming Continent-Ocean-Transition (COT) to reach its present shape (Fig. 6a).

In this part of the manuscript, we (i) hierarchize the importance of the different controlling parameters explaining the pockmarks locations and we discuss (ii) the fluid origin, (iii) the platform-scale circulation, (iv) the timing for pockmark activity as well as the (v) the probable triggering/enhancing mechanisms for fluid releases. The structural, physical, chemical and time modalities leading to the current-day observed abyssal physiography are also discussed.

5.1 Controlling parameters for pockmark regional distribution

https://doi.org/10.5194/se-2020-11
Preprint. Discussion started: 19 February 2020

358 **5.1.1. The distance to the BBE (first-order)**

359

360 All the discovered pockmarks are located at less than 4.7 km from the toe of the BBE, in this study
361 expressed by the isobath – 4000 m (Fig. 5b). 6 km is the width of the buried carbonate bench described in Schlager
362 et al. (1984) that is consistent with the amount of 5-6 km of erosional retreat proposed in Freeman-Lynde and Ryan
363 (1985). In this study, the 2D – seismic lines analysis corroborated that the aforementioned buried carbonate bench
364 is present all over the area and in particular underneath the studied giant pockmarks (e.g. Fig. 4d). These results
365 highlight the close genetic relationship between (i) the toe of the escarpment, (ii) the pockmarks occurrence and
366 (iii) the presence of carbonate bench. Moreover, an N-S elongated pockmark-underlying-seismic-anomaly (high
367 amplitude) appears to be located into the buried carbonate bench (e.g. Fig. 3b, 4b). Thanks to the high quality of
368 the acquired data, we here propose that the fluids at the origin of the studied abyssal giant pockmarks are currently
369 expressed by the recognized underlying high-amplitude seismic anomalies (Fig. 3c), and originate from the buried
370 carbonate bench.

371

372 **5.1.2 The regional faults (second-order)**

373

374 The highest density of pockmarks has been identified where the BBE is structurally controlled by the
375 Sunniland Fracture Zone (SFZ; Kindler et al., 2011), leading to the BBE curvature (23°30'0''N in figure 1b,
376 pockmarks #9 to #21 in figure 5a). This fact implies a causal connection between pockmarks location and structural
377 lineaments in which the focused fluid migration is much more effective than non-focused flow through matrix
378 porosities of the carbonate sedimentary column (Fig. 1; e.g. Abrams, 1992). The permeability of fracture corridors
379 in carbonates, so called structural porosity, is commonly higher than the matrix permeability (e.g. Rotevatn and
380 Bastesen, 2014); This is coherent with the preferential pathways used by the fluids to pop up of the buried bench
381 (Fig. 6b). Strike-slip faults are more efficient to drain fluids along a vertical direction (Cavailhes et al., 2013) that
382 is consistent with the SFZ inherited architecture which is considered as an inherited strike-slip tectonic structure
383 (transform faults) related to the Atlantic ocean opening. In addition, Privalov et al. (2019) showed that, at the plug
384 scale, dissolution and corrosion in carbonates are both eased and preferentially localized along fractures, along
385 which cavities more easily form and grow. These structural heterogeneities are here expressed at the big scale by
386 the structural lineaments that control the dissolution distribution at the platform scale.
387 The studied pockmarks show at least three morphometric similarities (i.e. diameter, water depth (- *4485*
388 *m; -4058 m)* and presence along a structural lineament) with the *plunge pools* succinctly described in Mulder et
389 al. (2018) (Fig. 1). These latter only differ in terms of (i) location in the geological system i.e., located into the
390 platform incising canyon and (ii) the depression depth (> 300 m). Unfortunately, we did not collect 2D seismic-
391 lines crossing the *plunge pools*. However, a partial explanation for *plunge pools* static emplacement into the canyon
392 (through times) could be the presence of an underlying cavity (doline-like feature) related to an underlying
393 structurally-controlled preferential dissolution/corrosion along a preexisting tectonic structure.
394 **5.1.3 Contourites, oceanic currents and buried sedimentary bodies (third-order)**
395 Pockmarks can be present whether contouritic deposits are present or absent, therefore demonstrating that
396 abyssal contouritic deposits did not inhibit the fluid-escape piercing at the toe of the BBE. In contrast, in the areas
397 where the contouritic deposits are absent (e.g. #9 to #21, Fig. 2c), the pockmarks number is higher than in the areas

https://doi.org/10.5194/se-2020-11
Preprint. Discussion started: 19 February 2020


Solid Earth
Discussions
Open Access
EGU

where the contourites are present (e.g. #1, Fig. 2a). In addition, the figure 4c shows that the pockmark #1 growth and probable related fluid-release both occur during a multi-stages building of contourite bodies. These observations would suggest that the contourites establishment (that is synchronous with the pockmark formation) has an impact on the pockmarks field development in controlling the numbers of pockmarks in a given area. This is consistent with the literature in which contourites are commonly considered as a seal for fluid escape structures (Sun et al., 2010). The studied pockmarks are elliptical in shape (Fig. 4) without any clear relation with the southwards stream bottom direction of the Deep Western Boundary Current (Meinen et al., 2013). This means that based on our data, abyssal currents did not modify the studied pockmarks geometric shapes (Andersen et al., 2008; Michel et al., 2017). Post-pockmark contourites may also hide some underlying buried pockmarks, not identified on neither 2D seismic lines nor on bathymetric map. Based on our 2D seismic analysis, no underlying buried sedimentary channels have been recognized underneath the abyssal mega-pockmarks of this study. This means that there is no additional buried sedimentary body at the origin of the storage and release of fluids with the exception of the carbonate bench.

5.2 Fluid origin and platform-scale circulation

5.2.1 Relation between the source depth and the pockmark diameter

The inner pockmarks mean diameters are smaller than the outer pockmarks ones (Fig. 5c). This observation suggests a particular geometric relation between the pockmark diameters and their distances to the BBE. Indeed, shallower the underlying source is located (overpressure location), smaller should be the pockmark diameter because the collapse structure is bounded by normal faults (Fig. 6b). In consequence, we propose that the top of the buried bench, trapping the fluids, exhibits its own eastwards dipping slope, probably acquired during the Oligocene erosion phase (Paull and Dillon, 1980). Assuming a similar pockmark collapse faults dips for all cases (either 60°, 70° or 80° in the figure 6d) and using the theorem of Pythagoras, we propose to quantitatively estimate the depth of the overpressure location for the inner pockmarks. The base of the seismic anomaly where the pockmark 1 roots is located at ~0.9 s below the seafloor i.e. 882 m - 1035 m in depth, assuming Vp velocities in the range of 1.96-2.30 km/s (Hollister et al., 1972a; Hollister et al., 1972b). These estimations seem consistent with a depth of ~ 1 km inferred from the 60° dipping normal faults (Anderson, 1951; Fig. 6c) commonly bounding collapsing structures such as sketched in usual pockmark models (Gay et al., 2017).

5.2.2 Fluid circulation at the Platform scale

The purpose of this section is to qualitatively describe and synthetize the architecture and the mechanisms of the fluid circulation in the Carbonate Bahama Platform (Fig. 7a). Surface seawater and meteoric waters both enter into faults and fracture corridors of the Bahamas platform hosting carbonates (limestone, dolomite) and evaporites (anhydrites, halites) (Fig. 7d). They form a ~1 km-deep meteoric aquifer in which part of the storage is matrix-located whereas freshwater supplies are most probably structurally guided; indeed, fresh water has been for instance recognized at ~3600 m of depth into the Great Bahama Bank (Walles, 1993; Fig.7a). Anhydrites such as the Cedar Key formation (Chanton et al., 1991) can be located at ~1 km depth into the platform (Hugues et al., 2007) and have a transitory barrier effect on the downwards fluid flow, efficiently compartmentalizing most of the fresh water aquifer circulation into the first kilometer. A fraction of this water dissolves these anhydrites,

https://doi.org/10.5194/se-2020-11
Preprint. Discussion started: 19 February 2020

increasing sulfates content in waters as well as water densities; this consequently enhances the water downwards movement into the Bahamas platform. These brines-rich waters ($SO4^{2-}$) are subsequently heated by thermal flux (e.g. 113°C at 4.6 km of depth; Chanton et al., 1991) generating formation of brines rich in sulfides (S^{2-}) and containing thermogenic methane (CH_4)(Fig.7b). These fluids migrate horizontally eastwards to the free edge of the Bahamian platform (~10.6 cm an^{-1}; Henderson et al.1999), along the relatively high-permeability faults and fractures systems (Fig. 7a; e.g., Sunniland Fracture Zone). In the BBE mixed water zone, the cold and oxygenated seawater microbially reduces sulfates (SO_4^{2-}) to sulfides (S^{2-}). Seawater and brines both keep on flowing through the structural heterogeneities, towards the bench, due their abnormal high density. They are subsequently "trapped" into the bench where the host-rock platform carbonates facies laterally and vertically changes to low-permeability hemipelagic deposits. This phenomenon results in an identified area of mixed chemistry (Fig. 7b) and relative fluid overpressure where the dissolution is probably over-developed (Corbella et al., 2004). The fluids are probably episodically expelled through the top of the bench - which is pre-fractured by the structural lineaments whereas its pressure occasionally exceeds the pressure of the overlying hemipelagics top-seal capillarity. A "doline-like-feature" takes place at the top of the carbonate bench (Oligocene A^u-unconformity), implying an overlying pockmark as a surface expression of fluid-escapes in fine-grained sediments (Fig. 7a). These energy-rich fluids may fuel chemosynthetic food chains such as shown in Chanton et al. (1991); however, we do not have any data for discussing such food chains in the study area. Fluid-escape features that have been recognized by Paull and Neumann (1987) are decametric in scale whereas the mega-pockmarks of this study are 10 to 100 times larger. This is consistent with the model of Gay et al. (2019) showing sporadic decametric seeps within a giant pockmark depression that act at different times as a function of available pathways in the sedimentary column and imply fluids lateral migration.

5.3 Timing of activity, triggering and enhancing mechanisms

During the CARAMBAR 2 survey, there was no evidence for acoustic anomalies in the overlying-pockmark water columns (#1 and #15). This suggests that no fluid was presently leaking from the pockmarks #1 and #15. However, the seismic anomaly recognized into the buried carbonate bench suggests that the fluids were present, at a non-evaluated pressure (Fig. 3c; 4c). As stated in the introduction, the following mechanisms probably play a role in a non-quantified proportion, at different times-scales enumerated as follows:

(i) At the geologic time-scale, Kohout convection drives the platform fluid circulation (Morrow, 1998). Modelling suggests that the inflow of seawater within carbonate platforms would be similar without the heat flux; however, this latter tends to reduce the asymmetry of circulation (Hughes et al., 2007).

(ii) At the Milankovich timescales, topography-driven flow can also enhance the platform circulation (Garven, 1995; Swennen et al., 2013) by the input of additional fresh water into the platform during the low-level stands (Hughes et al., 2007). Indeed, the large emerged Bahamas Platform (until/to -6000 years, Fauquembergue et al., 2018) probably supplied more fresh water in the underlying system than during the high sea level periods. This enhances the underlying dissolution by increasing chemical disequilibrium into the platform, implying significant source ratio changes in the underlying aquifer between brines, fresh water and meteoric waters. In

https://doi.org/10.5194/se-2020-11
Preprint. Discussion started: 19 February 2020


Solid Earth
Discussions
Open Access
EGU

addition, episodic fluid releases can also be directly related to the decrease of the overlying water column height above the pockmark during low level stands (Riboulot et al., 2014).

(iii) The erosion of the overlying contouritic body by an abyssal current, such as the WBUC (Meinen et al., 2013), can facilitate pockmark formation or activity. Indeed, the removal of this overlying material would change the pressure state of the underlying system (depressurization), therefore triggering a fluid release.

(iv) Earthquakes and volcanic eruptions occurrences have been correlated to tides (Kasahara, 2002) whereas their highest severity occurs when the tidal forces are the strongest (Glaser, 2004). Submarine earthquakes occurrence along deep mid-oceanic ridges (> - 2000 m) has been related to low tides when ocean loading is at a minimum (Tolstoy et al., 2002). The logic would be that fluids escaping from a pockmark-underlying chamber mechanically respond in the same way during low tides and associated depressurization. This has been corroborated for shallow water pockmarks affecting bioclastic carbonates where a relationship between seeps, tidal cycles and possibly atmospheric cyclonic lows is proposed (Rollet et al., 2006). The total water pressure generates a difference in interstitial pore pressure, which allows the expulsion of gas. However, for abyssal pockmarks, this pressure change could be negligible comparing to a pressure of 4500 m – high water column.

(v) Earthquake-induced circulation such as seismic pumping may have played a role in the system (Sibson, 1996). Earthquakes could also destabilize the hemipelagics top sealing properties by slope failures and submarine landslides (Masafero et al., 2011).

(vi) Quaternary tectonic tilting using the Sunniland Fracture Zone along the Bahama Escarpment (Kindler et al., 2011) may have reactivated faults and displaced spill points of the buried fluid traps, generating leaking of fluids.

6. Conclusions

This work details and quantifies the distribution, the morphology and the vertical architecture of 29 newly discovered abyssal giant pockmarks located at the toe of the BBE; Their origins and the mechanisms leading to their development are discussed consistently to the tectonic setting and the physiography of the area. The results and interpretations can be summarized as follows:

- Pockmarks are all giant (>250 m), abyssal (> 3000 m of water depth) and atypically occurs in carbonate settings below the CCD.
- Pockmarks are all located along the BBE, at less than 5 km from its toe (- 4000 m) and right above a buried carbonate bench related to the BBE erosional retreat.
- Pockmarks are preferentially located where the ocean-continent transition inherited structural lineaments controlling the Black Bahama Escarpment morphology intersect the > 4 km-high submarine carbonate escarpment (BBE).
- The BBE erosional retreat has preferentially reused the inherited faults, initially formed during the activity of the transforming ocean-continent transition (such as the Sunniland Fracture zone). Its present shape was mostly acquired by dissolution of carbonates by brines along tectonic structures.

https://doi.org/10.5194/se-2020-11
Preprint. Discussion started: 19 February 2020

- Fluids most probably circulate along the structural heterogeneities of the Bahamian platform, in response to the Kohout convection; Brine (sulfide-rich) formation is related to the dissolution of deep evaporite layers located ~1 km below the seafloor as well as geothermal heating. After oxidation nearby the BBE, the sulfites partially transform into sulphates. This oxidation reaction is indeed favoured by the inflow of oxygenized water through the fractured escarpment. The dense fluids are subsequently laterally trapped into the 5 km wide buried carbonate bench, surrounded by low-permeability hemipelagics, in which the dissolution is over-developed along fractures. The dissolution of the buried bench carbonates implies overlying collapse structures in the fine-grained deposits. In addition, when the critical pressure of the seal of the bench is exceeded, the fluids could be expelled via the bench top and form fluid-escape-features locally piercing fine-grained contourites.

7. Acknowledgements

We thank the captain and crew of the R/V *L'Atalante* for the quality of the acquired data, and Ifremer-Genavir (France) for cruise organization and technical support. We thank Mrs. XXXX and Mr. XXXX for their constructive reviews on this manuscript. We acknowledge IHS for granting University of Bordeaux with academic Kingdom® software licences.

8. References

Abrams, M.A. and Segall, M.P., Best practices for detecting, identifying and characterizing near-surface migration of hydrocarbons within marine sediments: Offshore Technology Conference in Houston, Texas, 2001. doi.org/10.4043/13039-MS.

Agirrezabala, L. M., S. Kiel, M. Blumenberg, N. Schäfer, and J. Reitner, Outcrop analogues of pockmarks and associated methane-seep carbonates: A case study from Lower Cretaceous (Albian) of the Basque-Cantabrian Basin, western Pyrenees: Palaeogeography Palaeoclimatology, Palaeoecology, 390, 94–115, 2013. doi: 10.1016/j.palaeo.2012.11.020.

Andersen, K. H., T. Lunne, T. J. Kvalstad, and C. F. Forsberg, Deepwater geotechnical engineering, Proc. XXIV National Conference of the Mexican Society of Soil Mechanics, Aguascalientes, 1–57, 2008.

Anderson, E.M., The dynamics of faulting and dyke formation with applications to Britain. Edimburgh., Oliver and Boyd, 206p, 1951.

Backshall, D.G., Barnett, J., Davies, P.J., Duncan, D.C. Harvey, N., Hopley, D., Isdale, P.J., Jennings, J.N. and Moss. R., Drowned dolines – the blue holes of the Pompey Reefs, Great Barrier Reef: Journal of Australian Geology & Geophysics, 4, pp. 99-109, 1979.

Bayon, G., Loncke, L., Dupré, S., Caprais, J.C., Ducassou, E., Duperron, S., Etoubleau, J., Foucher, J.P., Fouquet, Y., Gontharet, S., Henderson, G.M., Huguen, C., Klaucke, I., Mascle, J., Migeon, S., Olu-Le Roy, K.,

https://doi.org/10.5194/se-2020-11
Preprint. Discussion started: 19 February 2020

556 Ondréas, H., Pierre, C., Sibuet, M., Stadnitskaia, A., and Woodside, J., Multi-disciplinary investigation of fluid
557 seepage on an unstable margin: The case of the Central Nile deep sea fan: Marine Geology, 261, pp. 92- 104, 2009.
558
559 Betzler, C., Lindhorst, S., Hubscher, C., Ludmann, T., Furstenau, J., and Reijmer, J., Giant pockmarks in
560 a carbonate platform (Maldives, Indian Ocean): Marine Geology, 289, pp.1-16, 2011.
561 doi:10.1016/j.margeo.2011.09.004
562
563 Bleifnick, D.M., Robertson, A.H.F., and Sheridan, R.E., Deposition and provenance of Miocene
564 intraclastic chalks, Blake-Bahama Basin, western North Atlantic, in Initial reports of the Deep Sea Drilling Project,
565 Volume 44: Washington, D.C., U.S. Government Printing Office, p. 727-748, 1983.
566
567 Carlo, D-L., Characterization of rock-magnetic signature during subaerial exposure in Platform
568 Carbonates from new providence, Bahamas: PhD Thesis, Ohio state University, 66 p., 1996.
569
570 Cavailhes T., Sizun J.P., Labaume P., Chauvet A., Buatier B., Soliva R., Mezri L., Charpentier D., Leclere
571 H., Trave A., Gout C., Influence of fault rock foliation on fault zone permeability: The case of deeply buried
572 arkosic sandstones (Grès d'Annot, southeastern France), AAPG Bulletin, 97, 1521-1543, 2013. doi:
573 10.1306/03071312127.
574
575 Chanton, J.P., Martens, C.S., and Paull, C.K., Control of pore-water chemistry at the base of the Florida
576 escarpment by processes within the platform: Nature, 349, pp. 229-231, 1991.
577
578 Chapron, E., Van Rensbergen, P., De Batist, M., Beck, C., and Henriet, J.P., Fluid-escape features as a
579 precursor of a large sublacustrine sediment slide in Lake Le Bourget, NW Alps, France: Terra Nova, 16, pp. 305-
580 311, 2004. Doi: 10.1111/j.1365-3121.2004.00566.x
581
582 Cole, D., Stewart, S.A. and Cartwright J.A., Giant irregular pockmark craters in the Palaeogene of the
583 Outer Moray Firth Basin, UK North Sea: Marine and Petroleum Geology, 17 pp. 563-577, 2000.
584
585 Corbella, M., Ayora, C. Cardellach, E., Hydrothermal mixing, carbonate dissolution and sulfide
586 precipitation in Mississipi valley-type deposits: Mineralium Deposita, 39, p. 344-357, 2004. doi.10.1007/s00126-
587 004-0412-5
588
589 Dando, P.R., Austen, M.C., Burke Jr., R.A., Kendall, M.A., Kennicutt II, M.C., Judd, A.G., Moore, D.C.,
590 O'Hara, S.C.M., Schmaljohann, R. and Southward, A.J., Ecology of a North Sea pockmark with an active methane
591 seep: Marine Ecology Progress Series, 70, pp. 49–63, 1991.
592
593 Dawns, J.M., and Swart, P.K., Textural and geochemical alternations in late Cenozoic Bahamian
594 dolomites: Sedimentology, 35, pp.385-403, 1988.
595

https://doi.org/10.5194/se-2020-11
Preprint. Discussion started: 19 February 2020

596 Dickens, G. R., Rethinking the global carbon cycle with a large, dynamic and microbially mediated gas
597 hydrate capacitor: Earth Planetary Science Letters, 213, pp. 169-183, 2003.
598
599 Fauquembergue, K., Ducassou, E., Mulder, T., Hanquiez, V., Perello, M-C, Poli, E., Borgomano, J.,
600 Genesis and growth of a carbonate Holocene wedge on the northern Little Bahama Bank: Marine and Petroleum
601 Geology, 96, pp. 602-614, 2018. doi.org/10.1016/j.marpetgeo.2018.05.013
602
603 Foland, S., Maher, N., and Yun, J., Pockmarks along the California continental margin; implications for
604 fluid-flow, AAPG Bulletin, 83, 687-688, 1999.
605
606 Freeman-Lynde R.P., Cita, M.B., Jadoul, F., Miller, E.L., and Ryan, W. B. F. Marine geology of the
607 Bahama Escarpment: Marine Geology, 44, p. 119-156, 1981.
608
609 Freeman-Lynde R.P., and Ryan W.B.F., Erosional modification of Bahama Escarpment: Geological
610 Society of America Bulletin, 96, pp.481-494, 1985.
611
612 Garcia-Rios, M., Luquot, L., Soler, J.M., and Cama, J., Influence of the flow rate on dissolution and
613 precipitation features during percolation of CO2-rich sulfate solutions through fractured limestone samples:
614 Chemical Geology: 414, pp. 95–108, 2015.
615
616 Garven, Continental-scale groundwater flow and geological processes: Annual Review Earth Planetary
617 Sciences, 23, pp. 89-117, 1995.
618
619 Garven, H., and Freeze, R.A., Theorical analysis of the role of groundwater flow in the genesis of
620 stratabound ore deposits; 2, Quantitative results: American Journal of science, 284, 10, pp.1125-1174, 1994. doi:
621 10.2475/ajs.284.10.1125
622
623 Gay A., Lopez M., Cochonat P., Sultan N., Cauquil E. and Brigaud F., Sinuous pockmark belt as indicator
624 of a shallow buried turbiditic channel on the lower slope of the Congo Basin, West African Margin. In: Van
625 Rensbergen P, Hillis RR, Maltman AJ, Morley CK, eds. Subsurface Sediment Mobilization. Special Publications.
626 London: Geological Society of London, pp. 173–189, 2003.
627
628 Gay, A., Cavailhes, T., Grauls, D., Marsset, B., Marsset, T., Repeated fluid-expulsions during events of
629 rapid sea-level rise in the Gulf of Lion, western Mediterranean Sea: Bulletin de la Société Géologique de France,
630 188, 24, 2017. doi: 10.1051/bsgf/2017190.
631
632 Gay, A., Lopez, M., Potdevin, J-L, Vidal, V., Varas, G., Favier, A., and Tribovillard, N., 3D morphology
633 and timing of the giant fossil pockmark of Beauvoisin, SE Basin of France: Journal of the Geological Society, 176,
634 pp. 61-77, 2019. DOI: https://doi.org/10.1144/jgs2018-064.

https://doi.org/10.5194/se-2020-11
Preprint. Discussion started: 19 February 2020

635 Glaser, J.H., Breathing of the Seafloor: Tidal correlations of seismicity at Axial Volcano: Comment:
636 COMMENT: Geology, 31, 1, e3, 2004. doi.org/10.1130/0091-7613-31.1.e3
637 Gouze, P., Noiriel, C., Bruderer, C., Loggia, D. and Leprovost, R., X-ray tomography characterization
638 of fracture surfaces during dissolution: Geophysical Research Letter, 2003, 30, 5, pp. 1267, 2003. doi:
639 10.1029/2002GL016755
640
641 Heath K.C., and Mullins H.T., Open-ocean, off-bank transport of fine-grained carbonate sediments in the
642 northern Bahamas. In: Fine-Grained Sediments: Deep- Water Processes and Facies (Ed. by D. A. V. Stow and D.
643 J. W. Piper). Spec. Publ. Geol. Soc. Lond. Blackwell Scientific Publications, Oxford, 15, pp.199-208, 1984.
644 doi.org/10.1144/GSL.SP.1984.015.01.13
645
646 Henderson, G. M., Slowey, N., C., and Haddad, G., A., Fluid flow through carbonate platforms:
647 constraints from $^{234}U/^{238}U$ and Cl^- in Bahamas pore-waters: Earth and Planetary Science Letters, 169, pp.99-111,
648 1999.
649
650 Hollister, C.D., Ewing, J.I., Habib, D., Hathaway, J.C., Lancelot, Y., Luterbacher, H., Paulus, F.J., Poag,
651 C.W., Wilcoxon, J.A., and Worstell, P.: Deep Sea Drilling Program Volume XI, Shipboard Site Reports, Site 99,
652 Cat Gap, 1972a. doi:10.2973/dsdp.proc.11.102.1972
653
654 Hollister, C.D., Ewing, J.I., Habib, D., Hathaway, J.C., Lancelot, Y., Luterbacher, H., Paulus, F.J., Poag,
655 C.W., Wilcoxon, J.A., and Worstell, P.: Deep Sea Drilling Program Volume XI, Shipboard Site Reports, Site 100,
656 Cat Gap, 1972b. doi:10.2973/dsdp.proc.11.103.1972
657
658 Hornbach, M. J., C. Ruppel, and Van Dover C. L., Three-dimensional structure of fluid conduits
659 sustaining an active deep marine cold seep, Geophysical Research Letters, 34, 5, L05601,
660 doi:10.1029/2006GL028859, 2007.
661
662 Hugues, J.D., Vacher, H.L. and Sanford W.E., Three-dimensional flow in the Florida platform:
663 Theoritical analysis of Kohout convection at its type locality: The geological Society of America, 35, 7, pp. 663-
664 666, 2007. Doi: 10.1130/G23374A.1.
665
666 Kasahara J., Tides, earthquakes, and volcanoes: Science, 297, pp. 348–349, 2002.
667
668 Kindler, P., Godefored, F., Chiarada, M., Ehlert, C., Eisenhauer, A., Frank, M., Hasler, C-A., and
669 Samankassou, E., Discovery of Miocene to early Pleistocene deposits on Mayaguana, Bahamas: Evidence for
670 recent active tectonism on the North American Margin: Geology, 39, pp.523-526, 2011.
671
672 King, L. H., and MacLean, B., Pockmarks on the Scotian Shelf: Bulletin of the Geological Society of
673 America, 81, pp. 3141–3148, 1970.
674

https://doi.org/10.5194/se-2020-11
Preprint. Discussion started: 19 February 2020

675 Kohout, F.A., Henry, H.R., and Banks, J.E., Hydrogeology related to the geothermal conditions of the
676 Floridan Plateau: Florida Bureau of Geology Special Publication 21, p. 1-39, 1977.
677
678 Komatsu, G., Ori, G.G. Cardinale, M., Dohm, M.J., Baker, V.R., Vaz, D.A., Ishimaru, R., Namiki, N. and
679 Matsui, T., Roles of methane and carbon dioxide in geological processes on Mars: Planetary and Space Science,
680 59, pp. 169-181, 2011.
681 Maestro, A., Barnolas, A., Somoza, A., Lowrie, A., and Lawton, T., Geometry and structure associated
682 to gas-charged sediments and recent growth faults in the Ebro Delta (Spain): Marine Geology, 186, pp.351-368,
683 2002.
684 Marcon, Y., Ondréas, H., Sahling, H., Bohrmann, G., and Olu, K., Fluid-flow regimes and growth of a
685 giant pockmark: Geology, 42, 1, pp.63-66, 2014. doi:10.1130/G34801.1
686
687 Masafero, J.L., Bulnes, M., Poblet, J. and Eberli, G.P., Episodic folding inferred from syntectonic
688 carbonate sedimentation: the Santaren anticline, Bahamas foreland: Sedimentary Geology, 146, pp. 11-24, 2002.
689
690 Meinen, C., Johns, W., Garzoli, S.L., van Sebille, E., Rayner, D., Kanzow, T., Baringer, O., Variability
691 of the Deep Western Boundary Current at 26.5°N during 2004-2009: Deep-Sea Research II, 85, p.154-168, 2013.
692 doi.org/10.1016/j.dsr2.2012.07.036
693
694 Melim, L., and Masaferro, J-L., Subsurface geology of the Bahamas banks. In Vacher, H.L., Quinn,
695 T.M. (Eds), Geology and Hydrogeology of Carbonate Islands. Elsevier Science B.V, Amsterdam, Netherlands,
696 pp.161-182, 1997.
697 Micallef, A., Bernadt, C., and Debono, G., Fluid flow systems of the Malta Plateau, Central
698 Mediterranean Sea: Marine geology, 284, 1-4, pp. 74-85, 2011.
699 Michaud, F., Chabert, A., Collot, J-Y., Sallarès, V., Flueh, E.R., Charvis, P., Graindorge, D., Gustcher,
700 M-A. and Billas, J., Fields of multi-kilometer scale sub-scircular depressions in the Carbegie Ridge sedimentary
701 blanket: Effect of underwater carbonate dissolution: Marine Geology, 216, pp. 205-219, 2005.
702
703 Michel, G., Dupré, S., Baltzer, A., Ehrhold, A., Imbert, P., Pitel, M., Loubrieu, B., Scalabrin, C., Lazure,
704 P., Marié, L., Geldof. And Deville, E., Pockmarks on the South Aquitaine Margin continental slope: The seabed
705 expression of past fluid circulation and former bottom currents: Comptes Rendus Geoscience, 349, pp. 391-401,
706 2017.
707
708 Morrow, D.W., Regional subsurface dolomitization: models and constraints. Geoscience Canada 25, pp.
709 57– 70, 1998.
710
711 Mulder T., Gillet H., Hanquiez V., Ducassou E., Fauquembergue K., Principaud M., Conesa G., Le Goff
712 J., Ragusa J., Bashah S., Bujan S., Reijmer J.J.G., Cavailhes T., Droxler A.W., Blank D.G., Guiastrennec-Faugas
713 L., Fabregas N., Recouvreur A., Seibert C. Carbonate slope morphology revealing a giant submarine canyon (Little
714 Bahama Bank, Bahamas): Geology, 46, 31-34, 2018, doi: 10.1130/G39527.1.

https://doi.org/10.5194/se-2020-11
Preprint. Discussion started: 19 February 2020

715
716 Mulder T., Gillet H., Hanquiez V., Reijmer J.J.G., Droxler A.W., Recouvreur A., Fabregas N., Cavailhes
717 T., Fauquembergue K., Blank D.G., Guiastrennec-Faugas L., Seibert C., Bashah S., Bujan S., Ducassou E.,
718 Principaud M., Conesa G., Le Goff J., Ragusa J., Busson J., and Borgomano J., Into the deep: A coarse-grained
719 carbonate turbidite valley and canyon in ultra-deep carbonate setting, Marine Geology, 407, pp. 316-333, 2019.
720 doi: 10.1016/j.margeo.2018.11.003.
721 Mullins, H., Breen, N., Dolan, J., Wellner, W., Petruccione, J.L., Gaylord, M., Andersen, B., Melillo,
722 A.J., Jurgens, A.D., Orange, D., Carbonate platforms along the southeast Bahamas-Hispaniola collision zone:
723 Marine Geology, 105, 169-209, 1992.
724
725 Mullins, H. T., and Lynts, G.W., Origin of the northwestern Bahama Platform: Review and
726 Reinterpretation: GSA Bulletin, 88, pp. 1447-1461, 1977. doi.org/10.1130/0016-
727 7606(1977)88<1447:OOTNBP>2.0.CO;2
728
729 Ondréas, H., Fouquet, K.O, Charlou, J.L., Gay, A., Dennielou, B., Donval, J.P., Fifis, A., Nadalig, T.,
730 Cochonat, P., Cauquil, E., Bourillet, J.F., Le Moigne, M. and Sibuet, M., ROV study of a giant pockmark on the
731 Gabon continental margin: Geo-Marine letters, 25, 5, pp. 281-292, 2005.
732
733 Orange, D.L., Yun, J., Maher, N, Barry, J, and Greene G., Tracking California seafloor seeps with
734 bathymetry, backscatter and ROVs: Continental Shelf Research, 22(16), pp. 2273–2290, 2002.
735
736 Paull C.K., and Dillon, W.P., Erosional origin of the Blake Escarpment: An alternative hypothesis:
737 Geology, 8, pp. 538-542, 1980.
738
739 Paull C., and Neumann, A.C., Continental margin brine seeps: Their geological consequences: Geology,
740 15, pp. 545-548, 1987.
741
742 Paull, C.K., Spiess, F.N., Curray, J.R., Twitchell, D., Morphology of Florida Escarpment chemosynthetic
743 brine seep community sites: deep-tow, seabeam, and GLORIA surveys: Conference: Annual meeting of the
744 American Association of Petroleum Geologists, Houston, TX, USA, 20-23 March, 72, 2, 1988
745
746 Peterson, M.N. A., Calcite: Rates of dissolution in a vertical profile in the central Pacific: Science, 154,
747 pp. 1542-1544, 1966.
748
749 Pilcher, R., and Argent, J., Mega-pockmarks and linear pockmark trains on the West African continental
750 margin: Marine Geology, 244, pp. 15-32, 2007. doi:10.1016/j.margeo.2007.05.002
751
752

https://doi.org/10.5194/se-2020-11
Preprint. Discussion started: 19 February 2020

753 Privalov, V., Randi, A., Sterpenich, J., Pironon, J., and Morlot, C., Structural control of a dissolution
754 network in a limestone reservoir forced by radial injection of CO2 saturated solution; Experimental results coupled
755 with X-Ray computed tomography: Geosciences, 9, 1, 33, 2019.
756
757 Post, V. E.A, Groen, J., Kooi, H., Person, M., Ge, S. and Edmunds, W.M., Offshore fresh groundwater
758 reserves as a global phenomenon: Nature, 504, p.p. 71-78, 2013. doi:10.1038/nature12858.
759
760 Rollet, N.G.A.L., Kennard, J.M., O'Brien, P.E., Jones, A.T., and Sexton, M., Characterization and
761 correlation of active hydrocarbon seepage using geophysical data sets: An example from the tropical, carbonate
762 Yampi Shelf, Northwest Australia, Marine Petroleum Geology, 23, pp.145-164, 2006.
763
764 Rotevatn, A., and Bastesen, E., Fault linkage and damage zone architecture in tight carbonate rocks in the
765 Suez Rift (Egypt): Implications for permeability structure along segmented normal faults, in Spence, G.H., et al.,
766 eds., Advances in the Study of Fractured Reservoirs: Geological Society of London Special Publication, 374, pp.
767 79–95, 2014. doi: 10 .1144 /SP374 .1
768
769 Salmi, M.S., Johnson, H.P., Leifer, I. and Keister, J.E., Behavior of methane seep bubbles over a
770 pockmark on the Cascadia continental margin: Geosphere, 7, 6, pp. 1273-1283, 2011. doi: 10.1130/GES00648.1
771
772 Sanford, W., and Konikow, L., Porosity development in coastal carbonate aquifers: Geology, 17, pp. 249-
773 252; 1989.
774
775 Schlager, W., Austin. J. A., Jr., Corso, W., McNulty, C. L, Fluegel, E., Renz, O., and Steinmetz, J. C.,
776 Early Cretaceous platform re-entrant and escarpment erosion in the Bahamas: Geology, 12, pp. 147-150, 1984.
777
778 Shaw, J., Courtney, R.C., Currie, J.R., Marine Geology of Saint George's Bay, Newfoundland, as
779 interpreted from multibeam bathymetry and back-scatter data, Geo-Marine Letters, 17, pp. 188-194, 1997.
780
781 Sheridan, R.E., Conceptual Model for the Block-fault origin of the North American Atlantic Continental
782 Margin Geoscyncline: Geology, 2, 9, pp.465-468, 1974. doi.org/10.1130/0091-
783 7613(1974)2<465:CMFTBO>2.0.CO;2
784
785 Sibson, R., Structural permeability of fluid-driven fault-fracture meshes: Journal of structural Geology,
786 18, 8, pp.1031-1042, 1996. doi: 10.1016/0191-8141(96)00032-6.
787
788 Sultan, N., Marsset, B., Ker, S., Marsset, T., Voisset, M., Vernant, A.M., Bayon, G., Cauquil, E., Adamy,
789 J., Colliat, J.L. and Drapeau, D., Hydrate dissolution as a potential mechanism for pockmark formation in the
790 Niger Delta: Journal of Geophysical Research, 115, B08101, 2010. doi:10.1029/2010JB007453
791

https://doi.org/10.5194/se-2020-11
Preprint. Discussion started: 19 February 2020

Sun Q., Wu, S., Cartwright, J., and Dong, D., Shallow gas and focused fluid flow systems in the Pearl River Mouth Basin, northern South China Sea: Marine Geology, 1, 14, pp.315-318, 2012

Taylor, M.H., Dillon, W.P. and Pecher, I.A., Trapping and migration of methane associated with the gas hydrate stability zone at the Blake Ridge Diapir: new insights from Seismic data: Marine Geology 164, 79-89, 2000.

Tolstoy M, Vernon F L, Orcutt, J A, and Wyatt, F.K., Breathing of the seafloor: Tidal correlations of seismicity at Axial volcano: Geology, 30, pp. 503–506, 2002

Walles, F.E., Tectonic and diagenetically induced seal failure within the south-western Great Bahamas Bank: Marine and Petroleum Geology, 10, pp. 14-28, 1993.

Whitaker, F.F. and Smart, P.L., Active circulation of saline ground waters in carbonate platforms: Evidence from the Great Bahama Bank: Geology, 18, pp. 200-203, 1990.

Whitaker, F.F., and Smart, P.L., Circulation of saline groundwaters in carbonate platforms: A review and case study from the Bahamas. In: A.D. Horbury and A.G. Robinson (Editors), Diagenesis and Basin Development. Am. Assoc. Petrol. Geol. Studies Geol., 36, pp. 113-132, 1993.

Whitaker, F.F. Smart, P.L., Vahrenkamp, V.C., Nicholson, H. and Wogelius, R.A., Dolomitization by near-normal seawater? Field evidence from the Bahamas. In: B.H. Purser, M. Tucker and D.H. Zenger (editors), Dolomites, A volume in Honour of Dolomieu, International Association of Sedimentology Special Publication, 21, pp.111-132, 1994.

Wierzbicki, R., Dravis, J., Al-Aasnm, Harland, N., Burial dolomitization and dissolution of Upper Jurassic Abenaki platform carbonates, Deep Panuke reservoir, Nova Scotia, Canada: The American Association of Petroleum Geologists, 90, 11, pp. 1843-1861. 2006. DOI: 10.1306/03200605074

Wilson, A.M., Fresh and saline groundwater discharge to the ocean: A regional perspective: Water Resources Research, 41, W02016, doi:10.1029/2004WR003399, 2005.

9. Figure caption

https://doi.org/10.5194/se-2020-11
Preprint. Discussion started: 19 February 2020

Solid Earth
Discussions
Open Access
EGU

Figure 1

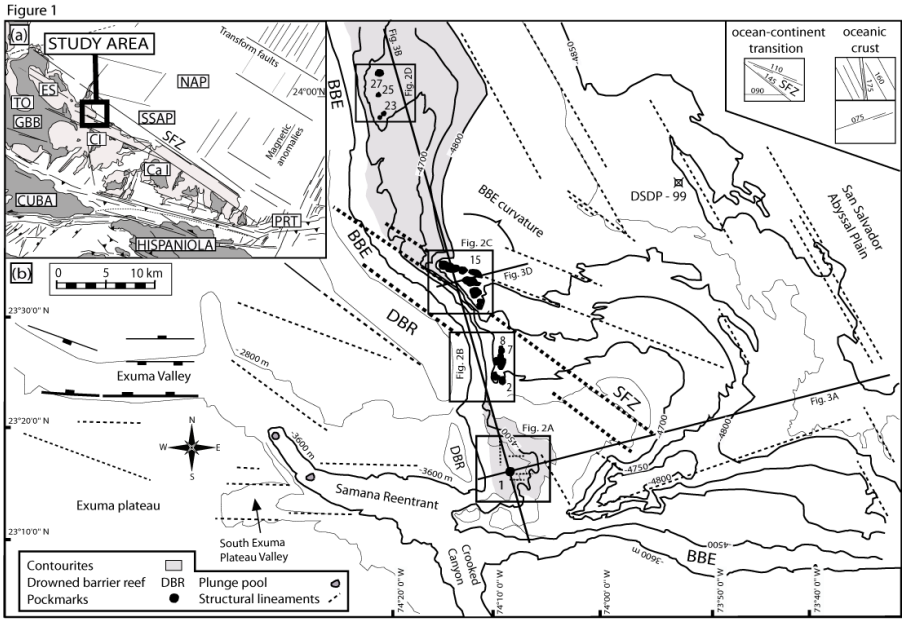

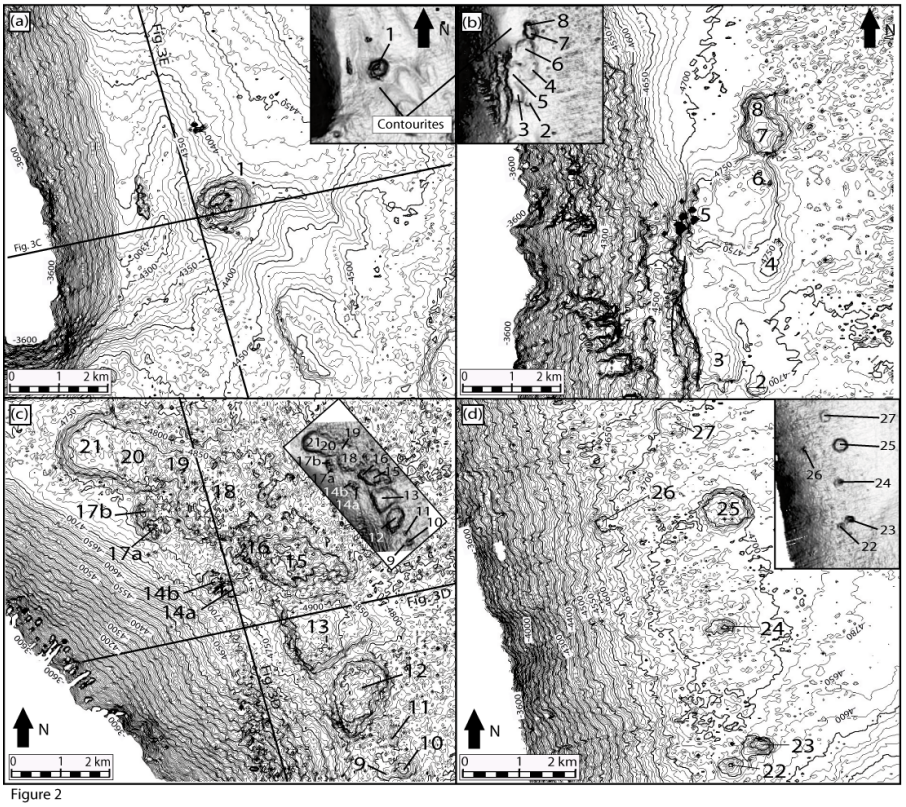

Figure 2

828
829
830

https://doi.org/10.5194/se-2020-11
Preprint. Discussion started: 19 February 2020

831 **Figure 1. (a) Structural Sketch of the Bahamas, Cuba and Hispaniola region. GGB -> Great Bahama Bank,**
832 **TO -> Tongue of the Ocean, ES -> Exuma Sound, NP, New Providence, LI, Long Island. SFOZ: Septentrional-Oriente**
833 **Fault Zone; NHF: North-Hispaniola Fault; SFZ: Sunniland Fracture Zone; NAP: North America Plate; CI Crooked**
834 **Islands; Ca I: Caicos Islands. SSAB: San Salvador Abyssal Plain. PPT: Puerto Rico Trench. Dark grey is used for both**
835 **platform water depth < 100 m, and the emerged areas. (b) Physiographic sketch in the Exuma Canyon area where all**
836 **the pockmarks of this study have been recognized; -3600 m isobath is located within the BBE slope.**
837
838 **Figure 2. (a) Details of the Pockmark 1 area where contourites are present. (b) Details of the pockmark 2 to 8**
839 **area where inner chains and outer chains appear. (c) Details of pockmarks 9 to 21 area within the BBE curvature where**
840 **inner and outer chains have been identified. (d) Details of the pockmark 22 to 27 area. Slope maps are also provided**
841 **for each bathymetric map.**
842
843
844
845
846
847
848
849
850
851
852
853
854

https://doi.org/10.5194/se-2020-11
Preprint. Discussion started: 19 February 2020

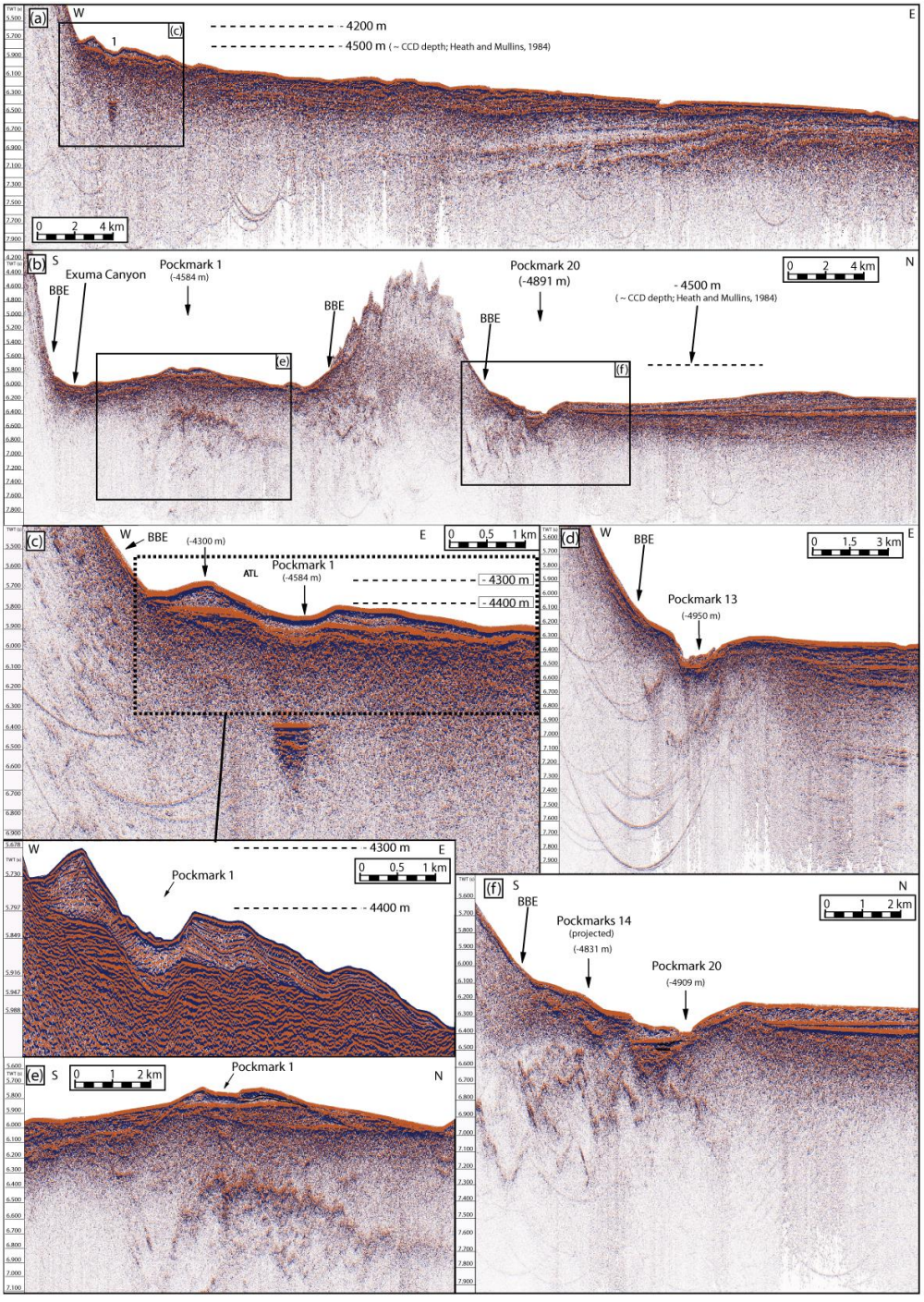

855

https://doi.org/10.5194/se-2020-11
Preprint. Discussion started: 19 February 2020

856 **Figure 3: 2D seismic lines TWT (s) of the study area: (a) N080 trending line respectively showing from the**
857 **west (left) to the east (right) the BBE, the pockmark #1 and the San Salvador Abyssal Plain. (b) N170 trending line**
858 **respectively showing respectively from the south (left) to the north (right), the Exuma Canyon, the pockmark #1, the**
859 **BBE, the pockmark #2 and the layered northern contouritic deposits. (c) Details of (a) showing the pockmark #1 with**
860 **its underlying seismic anomaly. (d) N080-trending line crossing the pockmark #13 in the BBE curvature area. (e) Details**
861 **of (b) showing the pockmark #1 with its related underlying seismic anomaly. (f) Details of (b) showing the pockmark 20**
862 **in the BBE curvature area. The aforementioned seismic lines are also reported in Figure 2.**
863
864
865
866

https://doi.org/10.5194/se-2020-11
Preprint. Discussion started: 19 February 2020

Solid Earth
Discussions
Open Access
EGU

867
868

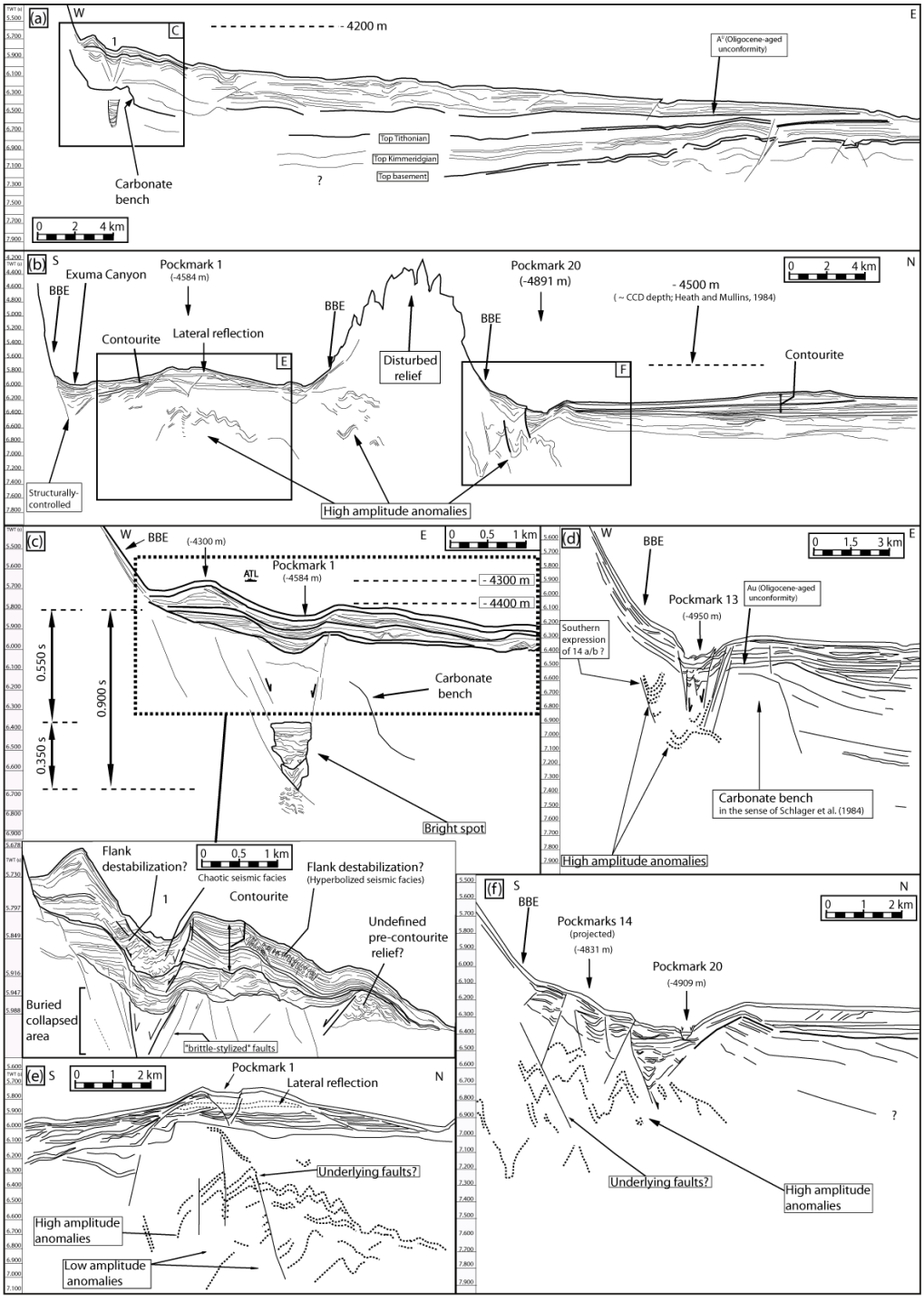

https://doi.org/10.5194/se-2020-11
Preprint. Discussion started: 19 February 2020

Solid Earth
Discussions
Open Access
EGU

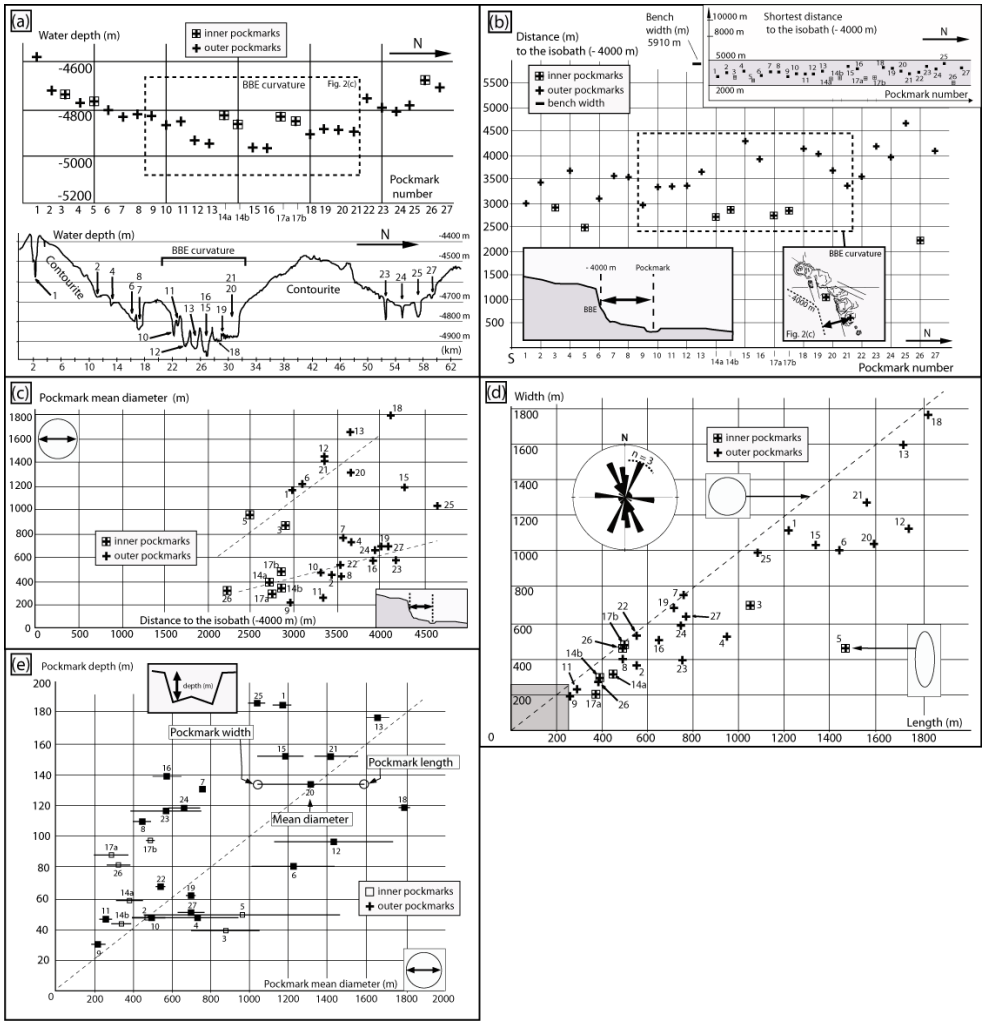

Figure 4: Interpreted 2D seismic lines of the study area: (a) N080 trending line interpretation showing the top basement, the top Kimmeridgian, the top Tithonian, the A^u unconformity and the post Miocene deposits. (b) N170 trending line interpretation showing the southern contouritic deposits where the pockmark #1 is located, the layered northern contouritic deposits and the pockmark underlying seismic anomalies. (c) Interpreted details of (a) showing the pockmark #1, piercing the contouritic deposits, the related underlying faults and seismic anomalies. (d) Interpreted N080 trending line crossing the pockmark #13 and showing the underlying seismic anomalies as well as the related collapse faults. (e) Interpreted details of (b) showing the lateral reflection within the pockmark #1 piercing the contouritic deposits as well as its underlying seismic anomaly. (f) Interpreted details of (b) showing the normal faults probably related to the pockmark formation in the BBE curvature area.

The aforementioned seismic lines are also reported in Figure 2.

https://doi.org/10.5194/se-2020-11
Preprint. Discussion started: 19 February 2020

884
885
886
887 **Figure 5: Graphs showing (a) the water depth for the 29 pockmarks of this study and a related S-N bathymetric**
888 **profile crossing the outer pockmarks. (b) S-N pockmarks numbering as a function of the distance to the BBE, here**
889 **expressed by the isobath (-4000 m). (c) Pockmark mean diameter as a function of the shortest distance to the BBE. (d)**
890 **Pockmark width as a function of pockmark length. Related rose diagram showing the elongation trend in the study**
891 **area. (e) Pockmark depth as a function of the pockmark mean diameter.**
892
893
894

https://doi.org/10.5194/se-2020-11
Preprint. Discussion started: 19 February 2020

Solid Earth
Discussions
Open Access
EGU

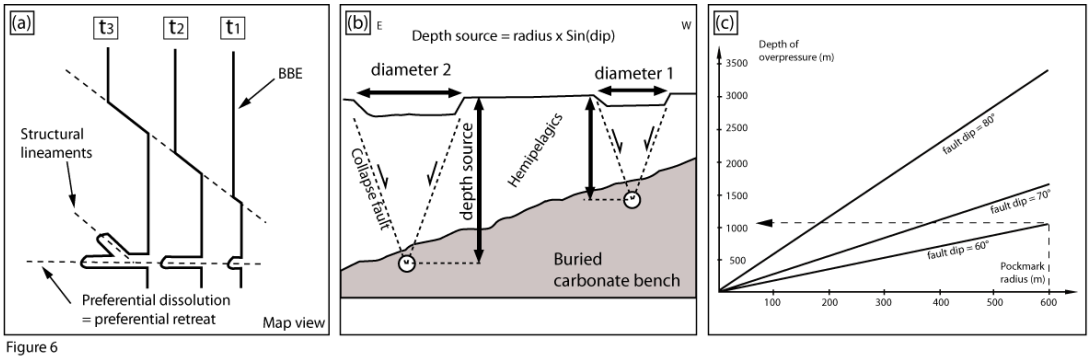

Figure 6

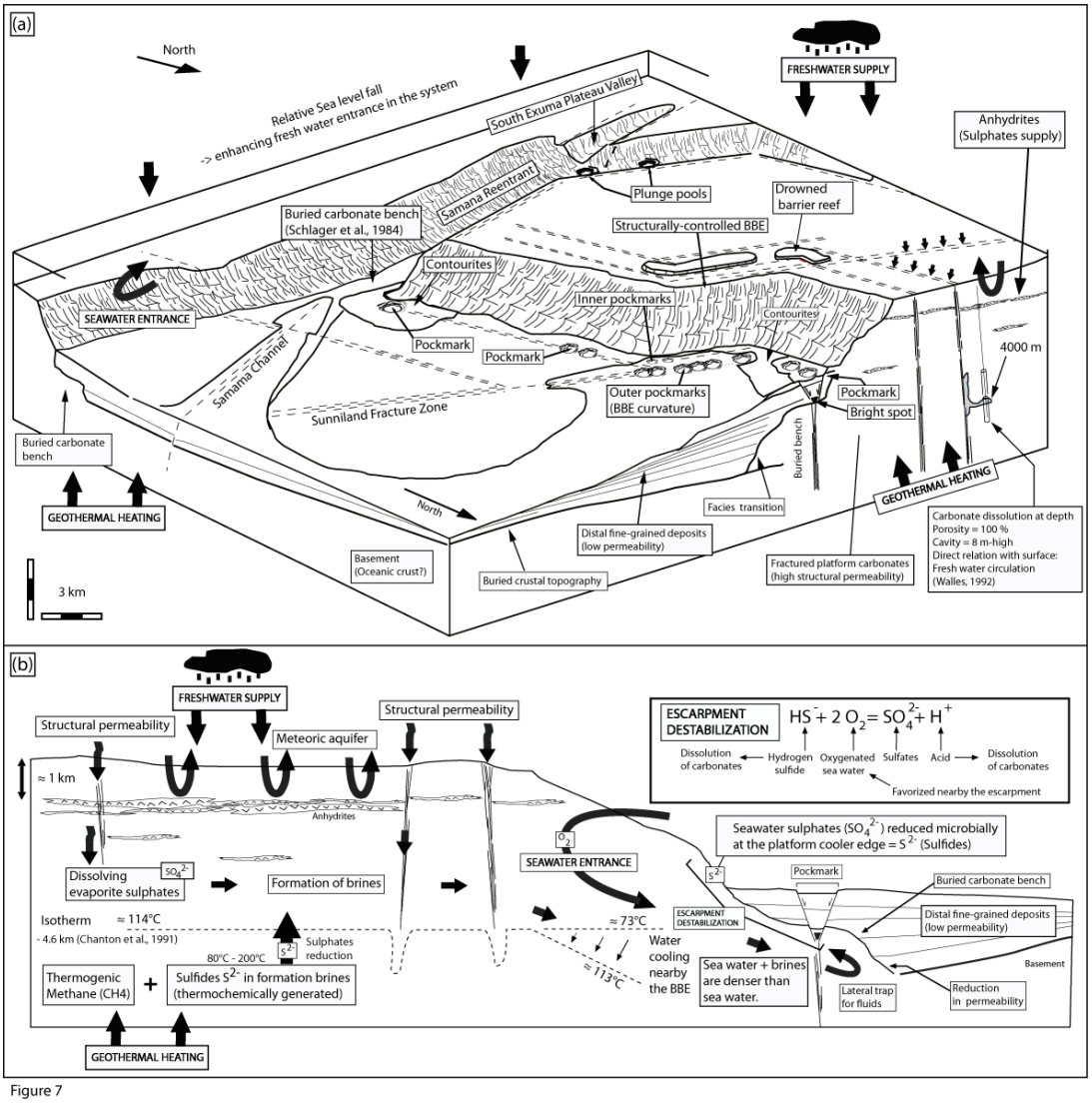

Figure 7

895

https://doi.org/10.5194/se-2020-11
Preprint. Discussion started: 19 February 2020

Solid Earth Discussions
Open Access
EGU

Figure 6: (a) Conceptual sketch showing how the BBE erosional retreat probably use the structural lineaments related to the TOC transition to reach its present-day physiography. (b) Conceptual sketch showing the relations between the depth of the fluid source and the radius of outer and inner pockmarks (c) Quantitative estimation of the overpressure depth in the case of pockmark 1.

Figure 7: (a) 3D block diagram expressing the general understanding of the system including our observations and the previous literature understanding. (b) 2D understanding of the system showing the importance of temperature, chemistry, and structural/sedimentological geometries.

POCKMARK NUMBER (From N to S)	WATER DEPTH (m)	POCKMARK DEPTH (m)	DISTANCE (m) TO THE ISOBATH "-4000 m"	LENGTH (m)	LENGTH (°N) ORIENTATION	WIDTH (m)	WIDTH (°N) ORIENTATION	MEAN DIAMETER (m)
1	-4584	184	2965	1213	42	1115	132	1164
2	-4722	47	3428	548	20	357	110	452,5
3	-4739	39	2894	1045	159	697	249	871
4	-4772	47	3650	940	25	520	115	730
5	-4771	49	2474	1461	179	454	269	957,5
6	-4803	80	3087	1433	24	1008	114	1220,5
7	-4841	130	3563	756	176	753	266	754,5
8	-4824	109	3538	489	85	396	175	442,5
9	-4834	30	2943	255	154	183	244	219
10	-4871	47	3307	487	170	455	260	471
11	-4851	46	3336	288	151	223	241	255,5
12	-4933	96	3341	1733	22	1125	112	1429
13	-4950	176	3638	1712	144	1599	234	1655,5
14a	-4830	58	2709	447	151	312	241	379,5
14b	-4866	43	2842	388	145	288	235	338
15	-4966	151	4268	1330	93	1034	183	1182
16	-4967	138	3898	643	36	500	126	571,5
17a	-4835	87	2736	371	162	198	252	284,5
17b	-4857	97	2838	495	72	470	162	482,5
18	-4909	118	4114	1819	168	1765	258	1792
19	-4886	61	4011	710	93	680	183	695
20	-4891	133	3648	1584	172	1038	262	1311
21	-4897	151	3339	1552	22	1273	112	1412,5
22	-4757	67	3525	547	60	527	150	537
23	-4797	116	4171	748	90	385	180	566,5
24	-4812	118	3928	741	95	581	185	661
25	-4785	185	4648	1075	118	993	208	1034
26	-4681	81	2211	381	8	266	98	323,5
27	-4710	50	4079	762	152	630	242	696

Table 1: Quantification of pockmarks attributes